POWER LOSS ANALYSIS OF N-PASHA CELLS VALIDATED BY 2D SIMULATIONS

G.J.M. Janssen[1], A. Gutjahr, A.R. Burgers, D. Saynova, I. Cesar, I.G. Romijn,
ECN Solar Energy, P.O. Box 1, NL-1755 ZG Petten, The Netherlands
[1]Phone: +31 224 56 4803; Fax: +31 224 56 8214; E-mail: janssen@ecn.nl

ABSTRACT: To reach >21% efficiency for the n-Pasha (passivated all sides H-pattern) cell of ECN, reliable power-loss analyses are essential. A power-loss analysis is presented that is based on experimental data but validated and completed by 2D simulations. The analysis is used to identify the key factors that will contribute most to achieving >21% efficiency.
Keywords: n-type, performance, simulation

1 INTRODUCTION

n-Pasha cells developed at ECN have shown a steadily increasing efficiency over the past few years with over 20% efficiency reported for cells made with industrial processing [1,2]. Further improvement is still both required and possible, but any experimental plan to achieve this must be based on a thorough analysis of the power-loss in present cells as well as reliable prediction of the impact of further modifications of cell architecture and process flow. A reliable power loss analysis, identifying the components and regions in the solar cell that limit the efficiency, is therefore required.

A power-loss analysis requires quantitative data of the cell on the optical properties, resistive properties, and recombination properties in the bulk, in the diffused layers, at the contacts and at the surfaces. Some of these data are experimentally well accessible, others are much more difficult to quantify. Moreover, consistency and transferability is required of these properties. This means that it may be assumed that these properties have similar values in different circumstances, e.g. in half-fabricates and finished cells. Numerical simulations in 1D or 2D are powerful tools to study the physical parameters mentioned above in a solar cell. However, the complexity and variety of the physical models used in numerical simulations necessitate good benchmarking and validation.

In this work first a breakdown of the efficiency loss of an n-Pasha solar cell is made on the basis of experimental data. The efficiency loss with respect to an ideal solar cell is divided into optical, recombination and ohmic contributions. Life-time data on half-fabricates and finished cells are then used to validate and parameterize the physical models for the different parts of the solar cell for 2D simulations. Full 2D cell simulations are carried out to assess the consistency of these data in the complete solar cell and refine the loss analysis. Finally, an outlook will be given on improvement of the n-Pasha efficiency with quantified targets.

2 n-PASHA DESIGN AND EXPERIMENTAL CHARACTERIZATION

2.1 n-Pasha design

The n-Pasha cell is a bifacial cell design on 6 inch n-type Cz material. Fig.1 shows the basic configuration of the n-Pasha solar cell. Both front and rear side feature H-grid metallization patterns. Yingli's Panda cells developed in collaboration with ECN and Tempress are based on this structure as well [3]. Both front and rear surface are textured, and coated with an antireflective SiN_x layer. On the front a BBr_3 diffused emitter is applied. The rear side features a lightly doped BSF based on $POCl_3$ diffusion. Under the contacts the BSF is higher doped. The group of cells on which the present loss analysis is based were processed on a 180 µm substrate with resistivity 2.7 ohmcm and stencil printed (front) or screen printed (rear) contacts. The total front side metallization including busbars covers 7.3% of the cell surface area.

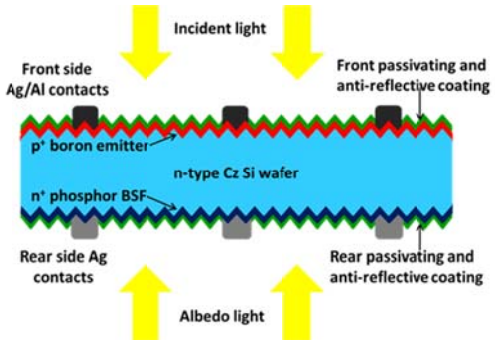

Figure 1: Cross section of the ECN n-pasha cell

2.2 Experimental characterization

IV curves with their characteristic values were extracted from measurements on full cells. Life-time and V_{OC}-implied measurements were done with a QSSPC Sinton 120 instrument on symmetrical ($p^+/n/p^+$) or asymmetrical ($p^+/n/n^+$) samples without metallization. Analyses were completed by Suns-V_{OC} measurements, spectral response and reflectivity measurements.

3 POWER-LOSS ANALYSIS BASED ON EXPERIMENTAL DATA

3.1 Main components

The performance of an ideal mono-junction c-Si solar cell would only be limited by intrinsic recombination in the bulk, by the maximum of the photogeneration which is limited by the Si bandgap and the fact that energies above this bandgap are lost by thermalization, and by the maximum fill factor of the resulting IV curve. As reference a cell with about 29% efficiency is used, corresponding with the photogeneration maximum for the AM1.5 spectrum of 46 mA cm^{-2}, an open circuit voltage V_{OC} of 745 mV, ideality factor n=1 and an ideal FF_0 of 0.85 [4].

Reflection by the front-side metallization of the n-Pasha cell covering 7.3 % surface area results in an equivalent reduction of the generated current, with associated small effects on the V_{OC} and maximum fill factor FF. The photogeneration is further reduced by reflection by the SiN_x covered part of the cell, by parasitic absorption, in particular in the SiN_x layers and free carrier absorption in the diffused layers of the cell, and by the escape reflectance, i.e. photons not absorbed after having bounced several times between front and rear surface. The direct reflection and escape reflection can be obtained from reflectivity measurements. The free carrier absorption was estimated from a model using the ECV diffusion profiles. The resulting data are collected in Table I: the optical losses not caused by the front-side metal reflection result in a further reduction of the photogeneration current by 2.6 $mAcm^{-2}$ and an associated small reduction in ideal FF and V_{OC}. The maximum power output after optical losses is calculated from $J_{ph}*V_{OC}*FF$.

Table I: Break-down of the efficiency loss. Data listed bold are measured values. The last column gives the loss in efficiency compared to the previous row

	J $mAcm^{-2}$	V_{oc} V	FF	Power $mWcm^{-2}$	Δη %ab
Maximum	46.0	0.745	0.85	29.25	
Metal reflection	42.6	0.743	0.85	27.02	2.2
Other optical	40.0	0.741	0.85	25.31	1.7
Recombi-nation	**39.1**	**0.651**	**0.81**	20.89	4.4
Ohmic	**39.1**	**0.651**	**0.78**	**19.84**	1.1

The actually measured J_{SC} is still below the estimated photogeneration current density, due to recombination at short circuit. The maximum expected power output including recombination can be calculated by $J_{SC}*V_{OC}*pFF$. The V_{OC} and J_{SC} values follow from the IV measurements, the pFF from a Suns-Voc curve. The pFF includes the deviation from the ideality factor n=1, as well as effect of shunt losses, which are expected to be negligible in optimized cells. The recombination losses constitute 4.4 % abs. loss of efficiency. The recombination losses occur in the diffused layers, at the contacts and in the bulk of the cell. A further breakdown of these losses is given in section 3.2.

The ohmic losses, finally, are calculated from the difference of the FF and the pFF according to: $\Delta P_{ohmic}=(pFF-FF)*V_{OC}*J_{SC}$. They seem to be the smallest contribution with only 1.1 mW cm^{-2}. The ohmic loss associated with lateral current transport ΔP_{lat} through a diffusion profile with resistivity R_{sheet} can be calculated from $\Delta P_{lat}=\frac{1}{3}R_{sheet}*(J_{MP})^2(L)^2$, with L the half-pitch of the cell and J_{MP} the current density at maximum power point MPP. Using the experimentally determined sheet resistances listed in Table II, and including the much smaller contribution of the transversal ohmic loss, the ohmic loss inside the silicon is estimated to be 0.8 mW cm^{-2} at MPP. This suggests that losses through the metallization series resistance and contact resistance of the metallization only contribute 0.3 mW cm^{-2} at MPP.

3.2 Breakdown of recombination losses

Recombination seems at present the largest contribution to the efficiency loss of an n-Pasha cell compared to an ideal cell. The recombination effects are from Auger and Shockley-Read-Hall recombination in the diffused layers, surface recombination, recombination at the contacts and recombination in the bulk. The latter is characterized by the bulk life time of the material, a value difficult to assess experimentally but believed to be in the order of 1 ms for the present n-type substrates with resistivity order 2.7 ohm cm. The recombination current in the bulk can then be written as:

$$J_{r,b} = \frac{qW\Delta n_b}{\tau} \quad \text{or} \quad J_{r,b} = \frac{qW\Delta n_b}{2\tau} \qquad (1)$$

for low level injection (LLI) and high level injection (HLI) conditions, respectively, with $\Delta n_b = \Delta p_b$ being the excess carrier density.

The other recombination processes can be characterized by J_0 values, the recombination current pre-factor. The J_0 value of a diffused layer, such as the emitter and BSF, will be made up of recombination in the layer, mainly Auger, and recombination at the surface of the layer. The recombination current density in such a layer is then defined by:

$$J_{r,d} = J_0 \frac{(p_0+\Delta n_b)(n_0+\Delta n_b)-n_i^2}{n_i^2} \qquad (2)$$

In this equation the excess carrier density Δn_b is the excess density just outside the diffused layer in the bulk.

J_0 values of the emitter and BSF were obtained from life-time measurements and are listed in Table II. The contact recombination current can be calculated with a similar approach, but J_0 values will differ from those of passivated layers due the higher recombination velocity at the metal and to the modifications in the diffused Si incurred when contacts are made.

Estimates of the J_0 for the contact regions are shown in Table II. Contact J_0 values were obtained by comparison of V_{OC}-implied on non-metallized samples and V_{OC} values of the finalized cell [5]. Values for the J_0 for the contact region include recombination in the diffused layer in the contact region (mainly Auger). For the emitter contact this contribution is small. On the other hand, the region under the BSF contact with a higher doping has a substantial contribution from recombination in the diffused layer, resulting in almost 40% of the J_0 value listed in Table II.

Table II: Measured J_0 and R_{sheet} values

	J_0 $fAcm^{-2}$	R_{sheet} $Ohmsq^{-1}$
Emitter	86	60
BSF	113	73
Emitter contact region	3000	
BSF contact region	1848	

N.B. J_0 values referred to $n_i=9.65\cdot10^9$ cm^{-3}

Eq. (1) and (2) show that the excess carrier density distribution in the cell has to be known in order to calculate the recombination currents in the different parts of the cell. A crude approximation for Δn_b, resulting in a uniform value over the cell, can be calculated from the cell voltage using the narrow base approximation [4]:

$$(p_0 + \Delta n_b)(n_0 + \Delta n_b) = n_i^2 \exp\left(\frac{qV}{kT}\right) \quad (3)$$

This results in Δn_b=3.9·10^{14} cm^{-3} at MPP and Δn_b=2.4·10^{15} cm^{-3} at $V_{OC,}$ respectively. Note, that for n-type wafers a resistivity of 2.7 ohmcm corresponds to a donor concentration of 1.7·10^{15} cm^{-3}. With these values, and applying the relevant area fractions for the BSF, emitter and contacts, the recombination currents are calculated according to (1) and (2). The breakdown of the total recombination current is given in Figure 2.

Figure 2 shows that both at MPP and V_{OC} the contacts and diffused layers have the largest contribution in the recombination, implying that they severely limit the cell efficiency. The differences in relative contributions at MPP and V_{OC} are due to the injection level that is closer to HLI at V_{OC} than at MPP. Fig 2 shows that the contact regions, which have a much smaller surface area than the passivated emitter and BSF, are responsible for a major part of the recombination current. This effect is most pronounced for the emitter contact. The front and rear passivated areas contribute almost equally to the recombination current.

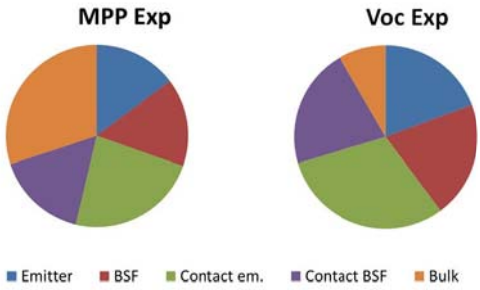

Figure 2: Breakdown of the recombination current at MPP and at V_{OC}, based on experimental data

4 NUMERICAL SIMULATIONS

4.1 J_0 calculations on diffused layers

Emitter and BSF both contribute substantially to the recombination loss. In order to establish whether this is due to surface recombination or Auger recombination, numerical simulations are required [6]. For this the Atlas package from Silvaco can be used [7]. A test structure is used which has a diffused layer on one side, as shown in Fig. 3. Illumination is from the rear, i.e. the non-diffused side, with monochromatic light with wavelength 500 nm.

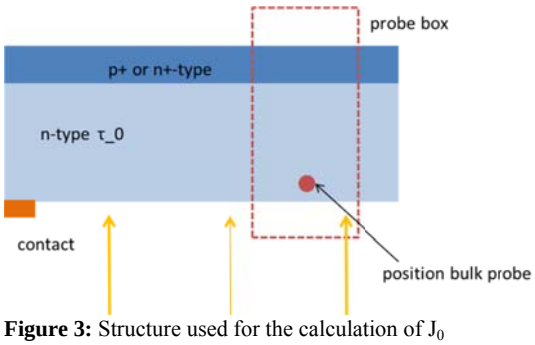

Figure 3: Structure used for the calculation of J_0

The J_0 of the diffused layer is then calculated from:

$$J_0 = R_{surf} \frac{qn_i^2}{\Delta n_b (N_D + \Delta n_b)} \quad (4)$$

R_{surf} is the recombination (Auger, surface recombination and Shockley-Read-Hall) in the n^+ or p^+ type layer averaged over the width of the probe box and Δn being calculated at the bulk probe.

The simulation is based on the diffusion profiles measured by ECV. In the n-Pasha cell the surfaces are textured. Including this texture in a simulation of a test structure in Fig. 3 or in the unit cell of a full cell would require very fine meshes and unacceptably long computing times. Compared to planar samples the surface area of a textured sample increases with a factor of 1.7, i.e. the volume of the layer increases with a similar factor. This implies that more Auger and surface recombination is taking place per unit cell surface than in a planar cell. As a first approximation the Auger parameters and the surface recombination SRV are multiplied by a factor of 1.7. Such an approach is only justified if the carrier concentrations are not seriously reduced by the enhanced recombination. Calculations have shown that the approach results in a textured : planar ratio of the J_0 of 1.5, which is an acceptable deviation of the assumed 1.7 ratio. This textured: planar ratio of 1.5 is in good agreement with simulated and experimental data in the literature [8,9].

For simulations on highly-doped structures Fermi-Dirac statistics must be used as well as a good model for the bandgap narrowing BGN [10]. According to the literature Schenk's BGN model physically the best one available [10,11]. For the Atlas simulations full implementation of this model is not yet available. Hence, we used the effective Klaassen BGN model [12]. Alternative software tools such as EDNA [13] can model J_0 with Schenk's BGN, for planar surfaces. For the present n-Pasha profiles we found similar qualitative behavior.

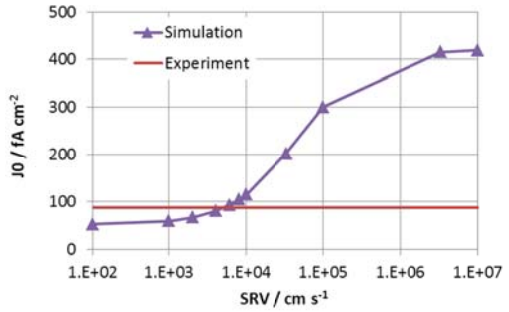

Figure 4: Calculated values of J_0 as a function of the SRV of the n-Pasha emitter. The experimental data value is represented by the horizontal red line.

Fig. 4 shows the calculated J_0 as a function of the assumed SRV of the n-Pasha emitter. The experimental J_0 value is plotted by a horizontal line. According to Fig 4, the calculated Auger limit of the emitter J_0 is about 50 fAcm^{-2}. The difference between this value and the experimentally determined J_0 is ascribed to surface recombination. Fig. 4 shows that SiN_x layer on the emitter clearly has a passivating effect, but the effective SRV at the interface is still in the order of 6000 cms^{-1},

contributing 34 fAcm^{-2} to the J_0 of the emitter. The Auger limit of the emitter seems to be in the order of 50 fAcm^{-2}. Notice, however, that both the calculated curve and experimental data have considerable uncertainties.

At the emitter contact the SRV would have the maximal value of $1 \cdot 10^7$ cms^{-1}, which in the simulation corresponds to a J_0 value of 420 fAcm^{-2}. This is much lower than the value of 3000 fAcm^{-2} estimated for the J_0 at the emitter contact in section 3. One reason for an increased J_0 would be that during firing of the contacts part of the diffused layer is etched away, thereby reducing the transport barrier for the minority carriers. Further contributions to the J_0 could come from increased SRH recombination due to defects introduced by the presence of metal inside the silicon or from non-smooth silicon/metal interfaces with higher effective interface area [14]. A description of the contacts including all these details is beyond the scope of this work. For simplicity we assume here that under the contact a uniform part of the emitter is etched away. This reduces the Auger recombination but the thinner p^+ emitter layer is a less effective transport barrier for electrons so at high SRV there is increase of the surface recombination, resulting in a high J_0. To attain the observed J_0 of the emitter contact it would have to be assumed that about 200 nm of emitter is etched away.

A similar study was done for the BSF, Fig. 5. In this case the calculated Auger limit is 62 fAcm^{-2}, which implies that the surface recombination contributes 51 fAcm^{-2}, with a SRV in the order of 10000 Scm^{-1}.

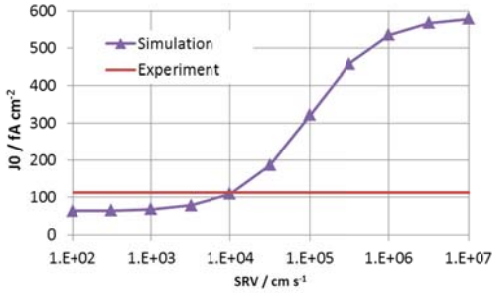

Figure 5: Calculated values of J_0 as a function of the SRV of the n-Pasha BSF. The experimental value is given by the horizontal red line

At the n-type contact a higher doped BSF is used. Like for the p-type contact at the emitter, it was found that by assuming that contact effectively etches away 200 nm, the J_0 agrees with the experimentally determined value.

4.2 Numerical simulation of the full cell

The simulations of the cell behavior were done on a 2D unit cell, with a width equal to a half-front side pitch. The same pitch was assumed at the rear with front and rear contacts exactly opposite each other. Note that the unit cell contains 50% of the full contact width. A fixed generation profile was used for the section of the cell under the passivated emitter. The profile was calculated with PC1D [15] and equivalent to 44.6 mA cm^{-2}. The calculation included effects of texturing and free carrier absorption.

The emitter and BSF were modeled as described in the previous section, with SRV values of 6000 and 10000 cms^{-1}, respectively. At the contacts an etch depth of 200 nm was assumed. The calculated IV-characteristics are shown in Table III, with a correction made for the inactive part of the cell covered by the busbars. Also a pseudo-IV curve was simulated for the 2D structure. The V_{OC} and J_{SC} show good agreement, the calculated efficiency is higher by 1.0 % abs than the measured one. This mainly due to a much higher (pseudo)FF.

The calculated pFF is higher by 1.4% abs. than the experimental pFF. This accounts for more than 0.3 % abs in efficiency loss. Differences in pFF may come from inhomogeneities in the full cell that are not included in the simulated unit cell. One cause could be edge recombination, which would increase the ideality factor.

The higher calculated FF is first of all related to the absence in the simulation of the ohmic resistance in the metallization. From comparison of the calculated values of FF and pFF a good estimate of the ohmic losses in the silicon can be obtained, i.e. (pFF-FF) $*J_{SC}*V_{OC}$, which results in 0.6 mWcm^{-2}. This is considerably lower than estimates in section 3. The difference can be associated with more efficient current paths and the injection level in the cell. As a consequence, it must be assumed that the metallization contribution and contact resistances that are not present in the simulation contribute in the order of 0.5 mWcm^{-2}, to account for the total ohmic loss observed experimentally.

Table III: Measured and simulated characteristics of n-Pasha cells

	Experiment	Simulation
J_{SC} (mAcm^{-2})	39.13	39.36
V_{OC} (V)	0.651	0.651
P_{MPP} (mWcm^{-2})	19.82	20.78
pFF	0.820	0.834
FF	0.779	0.811

A breakdown of the recombination current was also made for the simulations. This was done by integration of the recombination in the respective parts of the solar cell. The results are shown in Fig. 6. The breakdown at MPP and V_{OC} looks similar to the distribution obtained in section 3 based on experimental data, (Fig. 2) but with some notable exceptions.

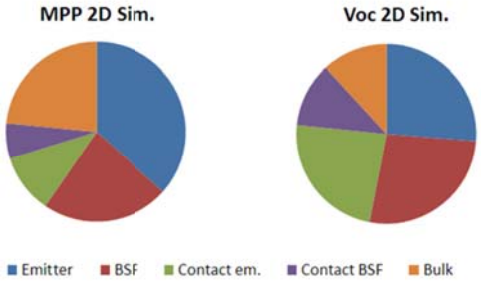

Figure 6: Breakdown of the recombination current at MPP and at V_{OC}, based on 2D simulations

In in the simulation the relative contributions of the contacts is smaller than in Fig. 2. This is a direct consequence of the non-uniform distribution of the excess carrier density, which at MPP is lowest near the contacts and highest in the region half-way between the contacts, as shown in Fig. 7. Note, that this effect was not taken into account when the J_0 values of the contacts

were estimated, i.e. the values in Table II are probably underestimations. The change in excess carrier distribution going from MPP to V_{OC} means that the relative contribution of the emitter contact at V_{OC} becomes larger than at MPP. The simulation results identify the emitter, BSF, and emitter contact as major sources of recombination.

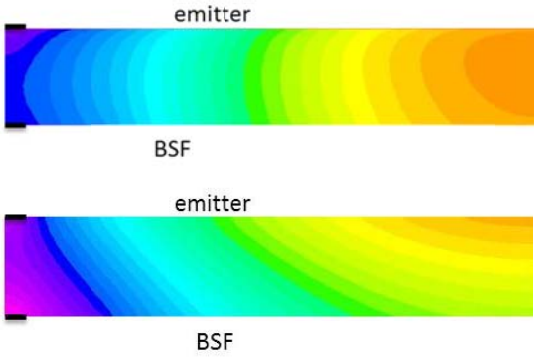

Figure 7: Distribution of the excess carrier density Δn_b in the bulk of the cell. Top: MPP, scale purple $1 \cdot 10^{14}$ to orange $4 \cdot 10^{14}$ cm^{-3}. Bottom V_{OC}, scale purple $2 \cdot 10^{15}$ to orange $2.6 \cdot 10^{15}$ cm^{-3}. The contacts are on the left-hand-side corners of the structure

5 DISCUSSION

The analysis of experimental data presented in Section 3 has indicated that recombination losses are the most important factor limiting the n-Pasha output. Further simulation results have shown that the diffused layers as well as the contacts contribute to this result, with the emitter contact, emitter and BSF being major sources of recombination. Simulations are required to distinguish between surface and Auger recombination. It was found that by improving the passivation of the non-metallized surfaces to S<1000 cms^{-1}, the recombination associated with the BSF and emitter can be reduced by almost 50%. An option to obtain near-to-perfect passivation may be for instance applying an ALD Al_2O_3 coating. Further reduction of J_0 can only be obtained by modifying the profiles to reduce Auger recombination, i.e. lower doping concentration. This would also require a deeper profile in order to keep the sheet resistances of the diffused layers at their present values.

The contact recombination is also large, and due to the non-uniform excess current density the emitter contact is especially limiting the V_{OC}. In the simulation the recombination at contacts was represented by an assumed etch below the contact, making the diffused layer a less effective transport barrier. This is an over-simplification. Still, to obtain a good contact there must be a transport barrier for minority carriers and this requires profiles with sufficiently high concentrations and sufficient depth. These profiles will differ from the profiles used in combination with ideal passivation, i.e. at the non-metallized surfaces. This implies that a selective emitter should be used.

The results of section 4.2 have shown that in order to correctly estimate the effect of modifying contacts and diffusion profiles J_0 values, an accurate estimate of the excess carrier density distribution must be used, i.e. a mere area-weighted estimate of J_0 values is not adequate**.** A more sophisticated analysis was made using the Quokka model [16], which calculates the excess carrier density but treats diffusions and contacts as conductive boundaries with recombination properties characterized by the appropriate recombination current pre-factor J_0. Some preliminary results obtained with this model are shown in Table IV. In order to gain 1.4 % abs. in efficiency target values for the passivated layers and contacts would be in the order of 20 and 200 $fAcm^{-2}$, respectively. An interesting observation is that by just improving the contacts only a limited gain is expected, but there is a large gain when this is done in combination with diffused layers.

Table IV: Calculated change in V_{OC} and η upon changing the recombination properties of in the n-Pasha cell. J_0 values are in $fAcm^{-2}$

Emitter J_0	86	20	86	20
BSF J_0	113	20	113	20
Em. Con. J_0	3000	3000	200	200
BSF con. J_0	1848	1848	200	200
ΔV_{OC}(mV)	0	20	12	41
$\Delta\eta$ (%abs.)	0	0.7	0.2	1.4

The results of section 3 and 4 have also shown that the ohmic losses in the n-Pasha cell are in the order of 1.1 Wcm^{-2}, 0.6-0.8 Wcm^{-2} of which is in the silicon. This emphasizes that any modifications of diffusion profiles should not lead to significant increase of the sheet resistance. The metallization including contact resistance seems to constitute only 0.3-0.5 Wcm^{-2}. Additional efficiency gain can be expected from reduction in inhomogeneities which may result from process inadequacies, such as non-uniform diffusions, or from edge recombination. However, they are as yet unspecified.

The front side metallization contributes 2.2 % abs. to the efficiency loss. There is limited gain expected from further reducing the width of fingers and busbars. A more substantial gain in current density would be obtained by adopting a MWT design.

Improved anti-reflection and improved trapping can contribute in minimizing the losses associated with direct rand escape reflectance. The use of lower diffusion concentrations in the emitter and/or BSF could reduce the free-carrier absorption.

6 CONCLUSIONS

A detailed loss analysis was made of an n-Pasha solar cell. This can to a large extent be done on the basis of experimental data such as IV characteristics, implied V_{OC}, lifetime time measurements, but 2D simulations are required for further accuracy.

The major loss factor is the recombination. J_0 data from lifetime measurements and V_{OC} implied data can be used to assign the recombination loss to different parts of the cell. Simulations are required to distinguish between Auger recombination and surface recombination of the diffused layers.

Further gain of efficiency to > 21% in the n-Pasha cell can be obtained with modified, well-passivated diffusions and improved contacts.

7 ACKNOWLEDGEMENT

AgentschapNL is acknowledged for financial support.

8 REFERENCES

[1] I.G.Romijn, J. Anker, A.R. Burgers, A. Gutjahr, B. Heurtault, M. Koppes, E.J. Kossen, M.W.P.E. Lamers, D.S. Saynova-Oosterling, and C.J.J. Tool, CPTIC 2013 (China PV Technology International Conference), Shanghai, China (2013).

[2] I.G. Romijn, A. Gutjahr, D.S. Saynova-Oosterling, J. Anker, E.J. Kossen, and C.J.J. Tool, Photovoltaics International (PV-Tech) 20 (2013) 33-40.

[3] A.R. Burgers, L.J. Geerligs, A.J. Carr, A. Gutjahr, D.S. Saynova-Oosterling, X. Jingfeng, L. Gaofei, X. Zhuo, W. Hongfang, H. Zhiyan, P. Venema, and A.H.G. Vlooswijk, 26th EUPVSEC, Hamburg, Germany (2011).

[4] M.A. Green, *Silicon Solar Cells: Advanced* Principles *& Practice*, The University of New South Wales, Sydney, NSW, 1995.

[5] T. Fellmeth, A. Born, A. Kimmerle, F. Clement, D. Biro, and R. Preu, Energy Procedia 8 (2011) 115-121.

[6] P.P. Altermatt, J.O. Schumacher, A. Cuevas, M.J. Kerr, S.W. Glunz, R.R. King, G. Heiser, and A. Schenk, J.Appl.Phys. 92 (2002) 3187-3197.

[7] Atlas, www.silvaco.com, (2013).

[8] S. Duttagupta, F. Lin, K.D. Shetty, A.G. Aberle, and B. Hoex, Prog.Photovolt: Res.Appl. 21 (2013) 760-764.

[9] F.-J. Ma, S. Duttagupta, M. Peters, G.S. Samudra, A.G. Aberle, and B. Hoex, Energy Procedia , in press (2013)

[10] P. Altermatt, Journal of Computational Electronics 10 (2011) 314-330.

[11] A. Schenk, J.Appl.Phys. 84 (1998) 3684-3695.

[12] D.B.M. Klaassen, J.W. Slotboom, and H.C. de Graaff, Solid-State Electron. 35 (1992) 125-129.

[13] K.R. McIntosh and P.P. Altermatt, 35th IEEE Photovoltaic Specialists Conference, Honolulu (2010) 002188-002193.

[14] E. Cabrera, S. Olibet, J. Glatz-Reichenbach, R. Kopecek, D. Reinke, and G. Schubert, J.Appl.Phys. 110 (2011) 114511-114515.

[15] D.A. Clugston and P.A. Basore, 26th IEEE Photovoltaic Specialists Conference, Anaheim (1997) 207-210.

[16] A. Fell, IEEE Transactions on Electric Devices 60 (2013) 733-738.